Free Volume Distributions in Glassy Polymer Membranes: Comparison between Molecular Modeling and Experiments

C. Nagel,[†] E. Schmidtke,[†] K. Günther-Schade,[†] D. Hofmann,[‡] D. Fritsch,[§] T. Strunskus,[†] and F. Faupel*,[†]

Technische Fakultät der Christian-Albrechts-Universität zu Kiel, Lehrstuhl für Materialverbunde, Kaiserstrasse 2, D-24143 Kiel, Germany, Institut für Chemie, GKSS Forschungszentrum GmbH, Kantstrasse 55, D-14513 Teltow, Germany, and Institut für Chemie, GKSS Forschungszentrum GmbH, Max-Planck-Strasse, D-21502 Geesthacht, Germany

Received May 17, 1999; Revised Manuscript Received December 14, 1999

ABSTRACT: We compare molecular modeling results of two glassy polymer membranes and one rubbery polymer membrane with gas transport parameters and free-volume-related quantities from positronium annihilation. A simple geometric model reveals hole size distributions of asymmetric shape. Among glassy polymers, the distribution parameters show a good correlation with average hole sizes determined by positron annihilation lifetime spectroscopy. Higher permeability is measured in the glassy polymer with the higher mean value of the hole size distribution. The permselectivity of the membranes for permanent gases can be interpreted in terms of the distribution broadness via free-volume-controlled diffusion selectivity. A comparison with the rubbery polymer shows that the permeation behavior is not determined only by the free volume concentration. The thermal fluctuations of the polymer matrix play an important role for gas transport properties.

1. Introduction

Polymer membranes have a wide industrial application; for example, to separate air for oxygen enrichment in combustion processes or nitrogen enrichment for prevention of oxidation. Removal of hydrogen from mixtures with nitrogen or hydrocarbons in petrochemical processing applications is another example.[1] For a given pair of gases *A*, *B*, there are two fundamental parameters characterizing membrane separation performance; these are permeability *P*, and the permselectivity $\alpha = P_A/P_B$, where *A* is the more permeable gas. The permeability is the product of gas flux and membrane thickness divided by the pressure difference across the membrane. Naturally, there is a tradeoff between *P* and α; that is, a polymer with high *P* has low α and vice versa. However, at a given permeability, selectivity may change by >1 order of magnitude due to different polymer structures. In recent years, a substantial research effort has led to polymers that are both more permeable and more selective (see, e. g., Mulder[2]). For a first characterization, permeation experiments are done using thick, homogeneous polymer films to measure transport properties directly. As a result, they give permeability *P* from the steady-state flux and diffusivity *D* from the time lag, which is the intersection of the linear extrapolation of the *p* versus *t* curve with the time axis (see, e. g., Mulder[2]). These macroscopic transport coefficients are essential for the characterization of the polymers but do not give much information on the atomic details unless the polymer structure is varied in a systematic way. This process is very laborious. Molecular dynamics (MD) simulations give valuable information on the microscopic transport process. Furthermore, they offer an opportunity to investigate polymer structures that are difficult (and therefore expensive) to synthesize.[3−5] However, at this time, molecular modeling still depends somewhat on experimental results as input. Another opportunity to get information on the atomic scale is positron annihilation lifetime spectroscopy (PALS). In PALS, the pick-off lifetime of the $^3S_1$ state of positronium (*ortho*-positronium, termed *o*-Ps in the following) is used to measure free volume hole sizes in polymers directly.[6] Free volume has been shown to have a strong influence in diffusion and permeation properties.[7−12] Even if the total free volume is constant, diffusivities can strongly depend on the local free volume between next neighbor chains.[13] In this paper, we compare results of the aforementioned three different methods used in practice. The aim is 2-fold. On one hand, the relations between gas transport and polymer properties such as hole size distributions and intermolecular forces are not yet completely understood. Here we will focus on the relations to hole size distributions. On the other hand, we will shed some light on what kind of information regarding free volume that PALS actually reveals. The results are based on permeation measurements, MD simulations, and PALS measurements on a set of two glassy polymers and one rubbery polymer.

2. Experimental Section

Synthesis of the polyimide (PI) and polyamidimide (PAI) polymers and the membrane samples, as well as the determination of macroscopic transport properties have been described in detail before[14,15] and will not be recalled here. The polydimethylsiloxane (PDMS) used was a two-component RTV silicone without any filler from Wacker (Germany). The structures of the repeating units are given in Figure 1.

By means of conventional X-ray diffraction (XRD), no indications of crystallinity could be found even after longer annealing experiments (several hours at $T > 300$ °C under 10^{-5} mbar vacuum). The glass transition

* Corresponding author.
[†] Technische Fakultät der Christian-Albrechts-Universität zu Kiel.
[‡] Institut für Chemie, Kantstrass 55.
[§] Institut für Chemie, Max-Planck-Strasse.

10.1021/ma990760y CCC: $19.00
Published on Web 03/01/2000

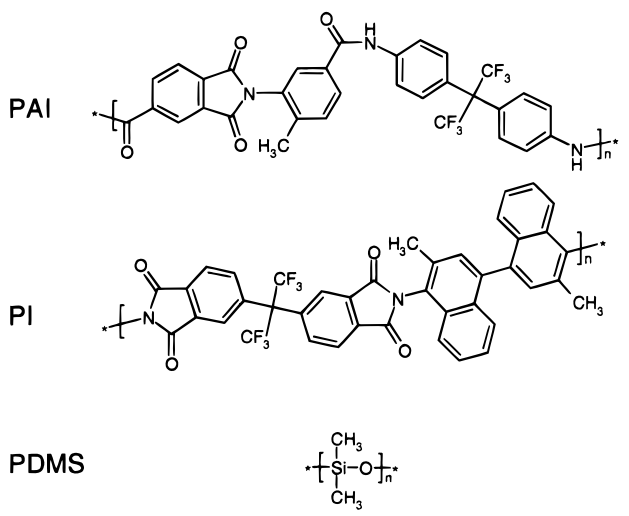

Figure 1. Repeating units of the polymers under investigation. See text for details.

Table 1. Characterization of the Polymer Membranes used in this study[a]

polymer		T_g [°C]	d [Å]	thickness [mm]
PAI	amorphous	355	5.5	0.150
PI	amorphous	403	6.3	0.058
PDMS	amorphous	−123[b]		0.626

[a] T_gs are tan δ-peak temperatures from DMTA ($\omega = 1.6$ s^{-1}, $\dot{T} = 2$ K min^{-1}) which have been corrected for a temperature gradient of the machine. In addition, d-spacings from XRD measurements and polymer film thicknesses are given. See text for details. [b] DSC, taken from ref 16.

temperatures were not easy to detect by differential scanning calorimetry (DSC), so dynamic mechanical thermal analysis (DMTA) was carried out at $\omega = 1.6$ s^{-1} and $\dot{T} = 2$ K min^{-1}. The α-peak temperature of tan δ was chosen as the glass transition temperature T_g. This T_g is somewhat higher (10−20 K) than the one determined by tangent construction on the modulus curve. The corresponding weight losses at T_g, determined by TGA, were <1% for PAI and ≃2% for PI. The results of the sample characterization are given in Table 1.

To get reasonable results with PALS, three effects had to be taken into account in the experiments. *First*, *o*-Ps lifetime may be decreased by "blocking" of holes by gas molecules.[17] If a cavity is already occupied by some molecule, the accessible volume for Ps is decreased or the cavity will not be occupied by Ps at all. In the case in which larger cavities are preferentially occupied by molecules (e. g., in the presence of size effects), the mean of the *o*-Ps lifetime distribution will be shifted to lower values. *Second*, the opposite phenomenon has been observed, too. In aliphatic polyamides, water absorption increases the *o*-Ps lifetime. In this case, the molecules may act as spacers.[18] *Third*, glasses are prone to irreversible structural relaxation upon annealing below T_g. Relaxation is accompanied by the decrease of free volume, which strongly affects the *o*-Ps lifetime. In particular, the PI showed a huge decrease of *o*-Ps lifetime upon annealing at $T > 150$ °C. To minimize the effects just mentioned (i.e., to guarantee comparability of the PALS and permeation results), all samples were treated appropriately. Before the PALS measurements, the samples were soaked in methanol and held in a vacuum at 110 °C to deaerate the film. The films are already tempered before the permeation measurements for ≃10 h at 110 °C. To prevent further relaxation, annealing before PALS was restricted to 1 h.

The positron sources (^{22}NaCl in aqueous solution) were directly deposited onto the sample surfaces. PAI and PI films were stacked to prevent annihilations from the surrounding media. Because only the longest lifetime was used for further analysis, no source corrections were carried out. The intensity of the source term was typically 4%. Tests with encapsulated sources did not reveal any significant influence in the long lifetime component.

Positron lifetime spectra were measured using a conventional fast−fast coincidence setup made of commercial Ortec components and Hamamatsu photomultipliers. The scintillator material was self-finished Bicron BC420. Counting rates of 300−400 s^{-1} have been achieved using a source activity of −30 μCi. The time resolution was determined with the program Resolution of the Patfit88 package.[19] We used directly deposited sources as well as sources encapsulated between Kapton foils (30HN, Du Pont). A variety of high-purity, well-annealed Al and Cu spectra with total counts between 3×10^6 and 12×10^6 were analyzed. Apart from the source term, fitting of one exponential convoluted with one Gaussian as a time-resolution function was sufficient to achieve good fits. The full width at half-maximum (fwhm) of the time resolution function was ≃229 ps.

For each polymer, 10−15 spectra containing total counts between 3×10^6 and 6×10^6 were measured. The spectra were decomposed into three discrete lifetime components using the Patfit88 package.[19] The longest lifetime was attributed to *o*-Ps pick-off annihilation (τ_{o-Ps}).

For the calculation of hole sizes, a simple quantum mechanical model[20,21] was used, which assumes the Ps atom to be confined to a spherical potential well with infinitely high walls. The assumption of spherical holes has been justified for flexible-chain polymers (polypropylene) as well as relatively stiff-chain polymers (bisphenol A-polycarbonate).[22] For the three polymers investigated in this study, validity of the assumption of spherical holes has been shown, too.[23] In the model just described, electron density of the surrounding molecules is approximated by an electron layer of constant thickness. The pick-off annihilation rate is assumed to be proportional to the probability to find the Ps atom inside the electron layer. This problem is solved by elemental quantum mechanics and yields

$$\tau_{o-Ps} = \lambda_0^{-1}\left(1 - \frac{R_h}{R_h + \delta R} + \frac{1}{2\pi}\sin\frac{2\pi R_h}{R_h + \delta R}\right)^{-1} \quad (1)$$

In eq 1, the prefactor is equal to the reciprocal spin-averaged Ps or Ps$^-$ annihilation rate.[24] Both values are equal to 0.5 ns. The quantities R_h and δR are the radius of the hole and an empirical parameter that describes the thickness of the electron layer, respectively. The value of δR has been determined before to be 1.656 Å by fitting eq 1 to positron lifetime values measured in systems of known hole sizes.[6] This model seems to be generally accepted and has been used by most authors, unless there were extremely aspheric holes.[25,26] As a result, eq 1 contains no free parameters at all, and the hole size can be directly calculated from the *o*-Ps lifetime. To prevent misunderstandings, this model is called the "standard model" in the following.

Because the *o*-Ps lifetime is expected to show a distribution in polymers, the discrete *o*-Ps lifetime obtained using the Patfit88 package actually represents a mean value. Thus, we use the terms "average *o*-Ps lifetime" for τ_{o-Ps} and "average hole radius" for R_h. The cavity volumes ("average hole sizes") were calculated from $V_h = 4\pi R_h^3/3$.

In this work, we have tried to extract hole size distributions from MD unit cells using a simple, purely mechanical model that relies on the following assumptions:

- The polymer matrix is completely frozen, and thermal fluctuations are neglected.
- All atoms are represented by hard spheres.
- The volume accessible to Ps can be approximated by a distribution of spheres that are placed into the rigid structure. In this way, the hole size distributions are actually distributions of cavity sizes accessible to Ps and therefore have a lower limit equal to the Ps radius r_{Ps}. The upper limit is given by the largest cavity of the unit cell. The radii of the polymer atoms as well as their positions are modeling results[3,4] and were given as text files. This model is called "sphere hole model" in the following. Refined models that take into account size and shape of holes were reported before.[27−29]

For the data evaluation we used the following algorithm. (1) Find the point $\vec{P}$ in the volume not occupied by polymer atoms that has the largest distance r_{max} to the boundary of the nearest atom. This distance should be larger than r_{Ps}. (2) Put $\vec{P}$ and r_{max} into a list. (3) Set a hard sphere with radius r_{max} onto the point $\vec{P}$ and disregard this place in the next run as occupied. (4) If $r_{max} \geq r_{Ps}$, return to (1); otherwise, stop.

3. Results and Discussion

From the overall chain structure of the polymers (see Figure 1), one can easily conclude that PAI and PI are very stiff-chain, high T_g polymers, whereas PDMS is known as a flexible-chain, low T_g material that is rubbery far below room temperature. This material was chosen for comparison. The bulky $C(CF_3)_2$ groups in the main chain as well as CH_3 substituents are known to increase chain stiffness, thereby reducing the packing density and hence increasing free volume and permeability. On the other hand, high chain stiffness permits high permselectivity. If there are additional interchain interactions (e. g., dipole interaction and/or hydrogen bondings), more energy is necessary to overcome attracting forces between chains. This effect also increases permselectivity. Because of the bulky naphthyl groups with attached methyl groups hindering the rotation around the imide bond, the PI has outstanding permeation properties as a glassy polymer. On the other hand, the PAI has a higher packing density, lower free volume, and hence lower permeability. Higher packing density naturally causes higher selectivity. In addition, hydrogen bonds may be formed in this material, which increase interchain interactions and, therefore, selectivity. In the PDMS, because of the flexible chains, selectivity for permanent gases is weak. However, permeability is high because the energy necessary to separate chains is very low. In the free volume picture, the cavities acting as diffusion vehicles can be redistributed without energy.

For each polymer, four independent unit cells have been analyzed in terms of the sphere hole model already outlined. The program was designed to report positions $\vec{P}_i$ and radii $r_{max,i} = R_i$ of each cavity i in an output file. From these data, we generated histograms for each unit cell and each polymer. The histograms are representations of hole size distributions (HSDs). These histograms are presented in Figures 2, 3, and 4 for PAI, PI, and PDMS, respectively. From these figures it can be seen that the HSDs are in no way symmetric functions but seem to diverge at small volumes and to approach zero at large volumes. This type of distribution was found

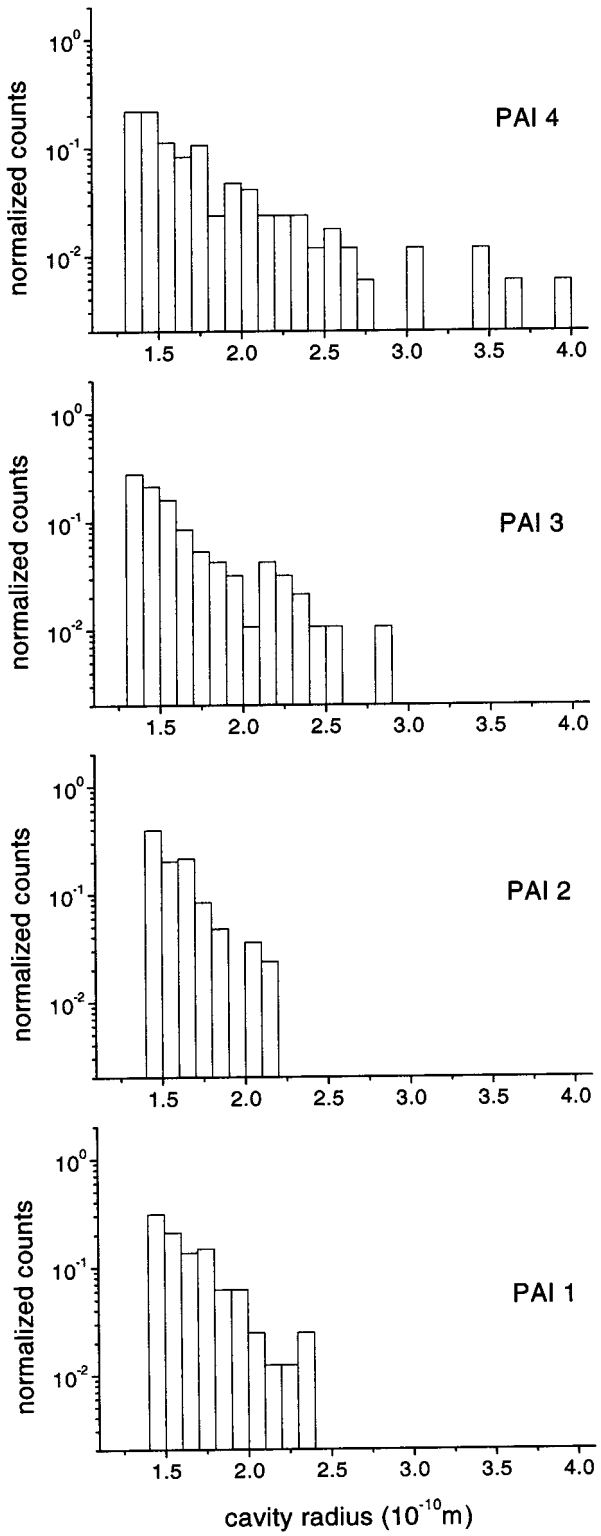

Figure 2. The HSDs according to the sphere hole model found in PAI. Normalized counts are plotted against cavity radii. Note the different behavior of PAI-3 and PAI-4.

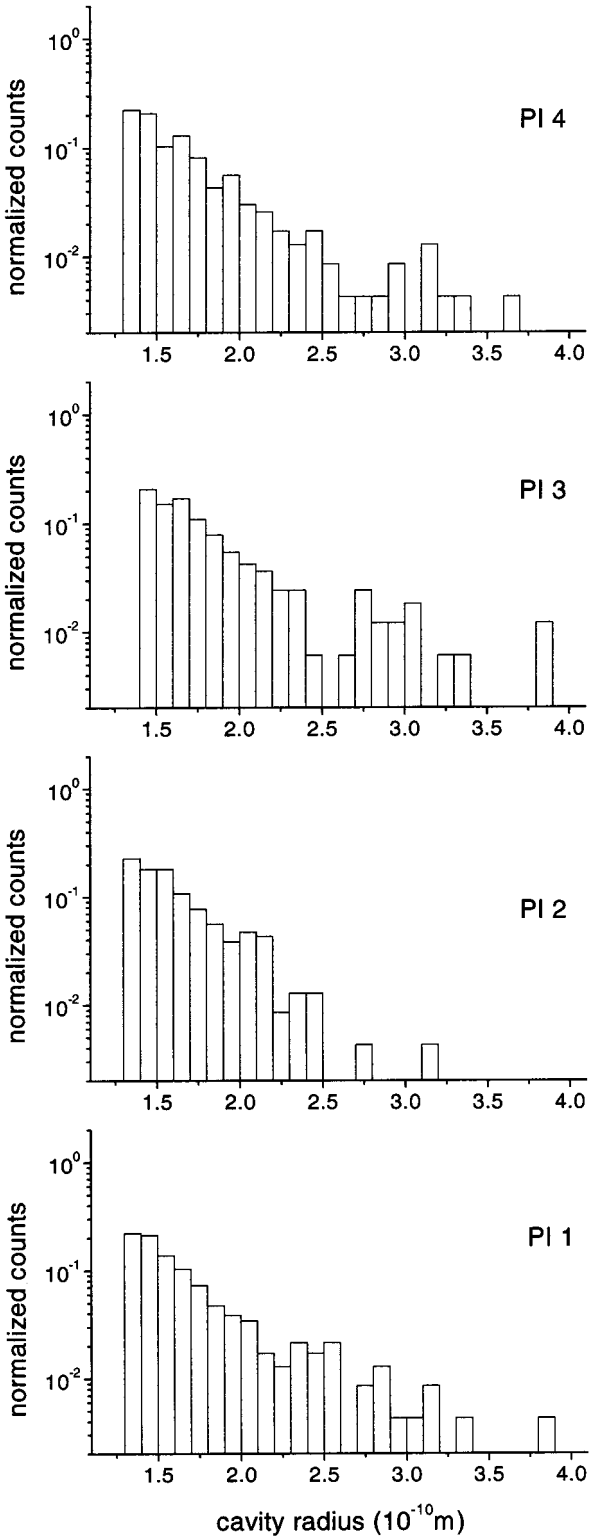

Figure 3. The HSDs according to the sphere hole model found in PI. Normalized counts are plotted against cavity radii.

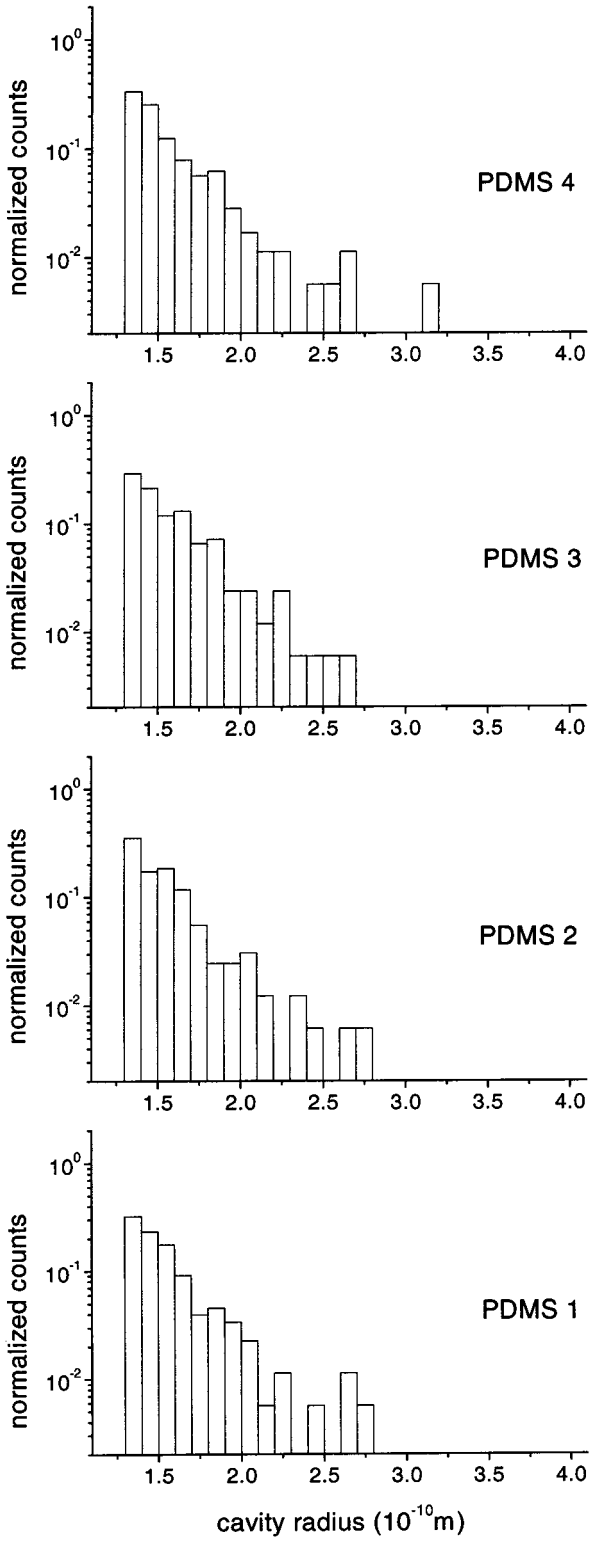

Figure 4. The HSDs according to the sphere hole model found in PDMS. Normalized counts are plotted against cavity radii.

in each unit cell. Clearly, the sphere hole model underestimates the volume of nonspherical holes. However, we do not expect that there is any influence in the general shape of the distributions.

The same type of asymmetric HSDs has been found before in other polymers using a different method.[22] The authors concluded that the shape of the distribution is a universal feature of polymers. In our opinion, this conclusion should be taken with caution because we cannot completely rule out statistical artifacts. As can be seen in Figures 2, 3, and 4, there are only a few counts in the region of large cavities. This result follows from the limited size of the unit cell. If one used a larger unit cell, the behavior in the large cavity region may become much different. However, because of the limited computing capability, it seems to be difficult to get larger unit cells at the moment. A similarly shaped HSD has been found in a metallic glass.[30] Peaks in the volume fraction of hole size distributions have been reported before.[27−29]

As can be seen in Figure 2, there are some irregularities in the broadnesses of the distributions. The unit cells PAI-3 and PAI-4 seem to have a few very large cavities. Unit cell PAI-4 actually has a percolating cavity[3,31] that cannot be seen with the sphere hole model (note the few counts at large cavities). Upon periodic continuation, this process would produce an infinitely large cavity. Accordingly, the MD simulations revealed abnormally high diffusion coefficients[3] for this unit cell. Also, unit cells PAI-3 and PAI-4 showed significantly larger solubilities than PAI-1 and PAI-2.[31] However, this increased solubility is probably an effect of the limited system size. A variance analysis gives different mean values at the 0.05 level for PAI-1−PAI-4 HSDs, whereas no difference has been found for the PDMS HSDs. For PI, variance analysis gives different means as well, but the effect is much less pronounced. This result may be taken as an additional hint for nonuniformity of the PAI HSDs. Because of these reasons, the PAI-3 and PAI-4 unit cells have been neglected when drawing physically relevant conclusions.

For comparison, the HSDs of each system have been mixed, giving a "mean" HSD including $N = \sum n_j$ cavities for each polymer system, where n_j is the number of holes in unit cell j, and j extends over the number of included original unit cells. This new HSD has to be related to a new unit cell of volume $V_{uc} = \sum v_{uc,j}$, where j extends over the number of included original unit cells and $v_{uc,j}$ is the volume of the unit cell j. For the mean HSDs, we have defined parameters that measure characteristic features of distributions. The quantity

$$\bar{V}_n = \frac{1}{N}\sum_{i=1}^{N} V_i \tag{2}$$

is the arithmetic mean of the HSD or number average hole size. Similar to molecular weight distributions,[32] the "volume average" hole size is

$$\bar{V}_v = \frac{\sum_{i=1}^{N} V_i^2}{\sum_{i=1}^{N} V_i} \tag{3}$$

Because the volume average is related to the variance, the uniformity

$$U = \frac{\bar{V}_v}{\bar{V}_n} - 1 \tag{4}$$

measures the broadness of the distribution. Further, the number density of holes has been defined as

$$N_0 = \frac{N}{V_{uc}} \tag{5}$$

The free volume fraction is the sum of all cavity volumes divided by the unit cell volume:

$$v_f = \frac{\sum_{i=1}^{N} V_i}{V_{uc}} \tag{6}$$

Table 2. Parameters of the Mean HSDs Obtained from Application of the Sphere Hole Model to Unit Cells from Molecular Modeling[a]

polymer	PAI	PAI[b]	PI	PDMS
N_0 [10^{21} cm^{-3}]	4.2	3.7	6.2	5.9
$\bar{V}_n$ [Å^3]	22.5	17.2	23.1	16.0
$\bar{V}_v$ [Å^3]	109.4	20.4	50.2	24.3
U	3.9	0.2	1.2	0.5
v_f [%]	9.4	6.4	14.4	9.5
V_h [Å^3]		140	280	321
I_3 [%]		3	21	43
P_{H_2}		33	550	670
P_{He}		38	340	390
P_{O_2}		2.8	140	580
P_{CO_2}		15	960	2800
α_{H_2/N_2}		72	15	2.5
α_{O_2/N_2}		6.1	3.8	2.2
α_{H_2/CH_4}		130	14	0.80
α_{CO_2/CH_4}		60	24	3.4

[a] If not stated otherwise, all 4 unit cells of each polymer under investigation were taken into account. In addition, the results of the PALS measurements as well as the permeabilities P (in barrers; 1 barrer = 1 Ba = 10^{-10} cm^3 (STP) cm/cm^2 s cmHg) and permselectivities α are given. The V_hs were determined using the standard model. See text for details. [b] PAI-3 and PAI-4 neglected.

Table 3. Parameters of the Mean HSDs Obtained from Application of the Sphere Hole Model to Unit Cells from Molecular Modeling taking into Account Clustering[a]

polymer	PAI	PAI[b]	PI	PDMS
N_0 [10^{21} cm^{-3}]	2.4	3.1	2.8	3.7
$\bar{V}_n$ [Å^3]	38.9	21.0	51.5	26.0
$\bar{V}_v$ [Å^3]	608.8	29.8	651.3	89.2
U	14.7	0.4	11.6	2.4
v_f [%]	9.4	6.4	14.4	9.5

[a] Note the right-shift distribution. [b] PAI-3 and PAI-4 neglected.

All parameters describing the HSDs of the different polymers investigated are given in Table 2. Additionally, we have included the data obtained in the case in which all unit cells of the PAI are taken into account. Apart from the distortions caused by PAI-3 and PAI-4, from Table 2 it can be seen that PAI has a smaller average hole size, fewer sites to be occupied by penetrant molecules, and a smaller HSD than PI. This observation is in good agreement with the PALS results: The PAI has a smaller V_h than PI. The measured *o*-Ps intensity I_3 is sometimes related to the number of sites available to Ps. However, I_3 is also influenced by other factors, like formation probability of Ps, which depends on the specific mechanism of slowing down of the positron. Despite this fact, in the systems considered here, the behavior of I_3 roughly fits the picture that PAI has fewer sites available to Ps.

The absolute values of $\bar{V}_n$ and V_v on one hand and V_h on the other are not comparable at all. The parameter V_h is 8−12 times larger than $\bar{V}_n$ and 6−7 times larger than V_v. There are three possible explanations for this fact. First, there is a shortcoming of the sphere hole model: trying to place spheres into the matrix always underestimates the cavity volume because of irregularities. However, this effect alone cannot explain the large discrepancies. Taking into account clustering of adjacent spheres by replacing them with one cavity volume equal to the sum of all volumes of the spheres belonging to the cluster results in a right-shift of the HSDs. The results are given in Table 3. However, these corrections are limited in accuracy and are therefore well-suited only for illustrative purposes. Second, we cannot exclude

an accumulation of large volumes around a mean value that could appear at high counting statistics. Due to the limited system size (cf., Figures 2, 3, and 4), there are only a few counts at large cavity sizes instead. A peak at large volumes in the HSD would lead to a higher mean value. In addition, we do not know which part of the HSD really takes part in the diffusion process. A subdivision of the HSD into "interstitial" free volume and "cavities" may be necessary. In this case, the arithmetic mean of the HSD would not be a good measure for comparison with permeation and PALS. Unfortunately, currently we are not able to test this. Third, there are fewer data on how Ps occupies the cavities. There are hints in the literature[33] that Ps preferentially resides in large cavities (defects), like vacancies in molecular crystals. If, similar to molecular crystals, Ps detects only a few large holes in glassy polymers, this preference would lead to overestimating the calculated HSD mean value by PALS. This overestimation has also been found comparing diffusivities of small molecules in glassy polymer membranes with PALS measurements.[34] Hence, we conclude that this explanation is also reasonable.

So far, we have left out the PDMS data from the discussion, mainly because the first assumption in the sphere hole model is less justified in the case of PDMS. Judging from the chain structure as well as from MD,[35] local chain flexibility is much higher in PDMS than in the glassy polymers PAI and PI. Also, the low T_g indicates long-range chain mobility. Because dynamics is completely neglected in the sphere hole model, freely fluctuating free volume elements acting as diffusion vehicles are disregarded. Especially in the case of rubbery polymers, the static model is not well suited to describe permeation. In the MD simulations,[31,35] it can directly be seen that the thermal fluctuations of the polymer matrix are strongly involved in the diffusion process. The fluctuations occur on a much shorter time scale in the PDMS[35] than in PAI and PI. Comparing the HSD parameters with the overall trend in Table 2 clearly shows that the permeability cannot be explained by static free volume in rubbery polymers.

From Table 2, one notes that the experimentally determined average hole sizes V_h and permeabilities P are correlated, whereas both V_h and HSD parameters as well as P and HSD parameters are not correlated (the explanation has already been given). From this result we conclude that Ps is able to detect the fluctuating part of the free volume, too. Probably, the Ps itself is mobile, like a diffusing gas molecule. In fact, experiments[36,37] reveal a Ps diffusion constant of $10^{-6}-10^{-4}$ $cm^2\ s^{-1}$, which is higher than or comparable to helium diffusion constants in the polymers under investigation: $D_{PAI}^{He} = 5.5 \times 10^{-6}\ cm^2\ s^{-1}$, $D_{PI}^{He} = 2.3 \times 10^{-5}\ cm^2\ s^{-1}$, $D_{PDMS}^{He} = 9.0 \times 10^{-5}\ cm^2\ s^{-1}$ (time-lag, 500 mbar, 30 °C). Obviously, V_h determined by PALS reflects the real transport behavior better than the picture of static free volume mainly because Ps detects the dynamics of the polymer matrix, too.

The permselectivities α are given in the last lines in Table 2. One notes that α is high for PAI, whereas α is lower for PI. This difference is in accordance with what one would expect from the polymer structures, as already discussed. Comparison of α of the glassy polymers PAI and PI with their HSD parameters suggests that higher permselectivity is related to narrower distributions. If permselectivity is governed by *D*-selectivity, as is the case for small gas molecules, then this phenomenon can be interpreted by reduced diffusivity for larger gas molecules due to the reduced number of larger cavities. This mechanism is valid for H_2, He, N_2, and O_2. For CO_2 and CH_4, *S*-selectivity might become important, too. Because of their critical temperatures, these gases naturally have higher solubilities. In the picture of Langmuir sorption, the influence of the HSD may become important even in this case. At narrow distributions, one would expect less solubility for larger gas molecules and hence higher *S*-selectivity. In PDMS, *D*-selectivities are naturally very low due to the high chain flexibility. Because Langmuir-type sorption behavior is not expected in polymers above T_g, no relation between *S*-selectivity and HSD parameters can be obtained. As a consequence, *P*-selectivity is weak in this material and no correlation between *P*-selectivity and HSD broadness is to be expected.

4. Conclusion

We have compared the results of positron annihilation lifetime spectroscopy, molecular modeling, and time lag measurements that are frequently used in membrane research. A static-free volume model that has been applied to three different modeled polymers revealed asymmetric, decreasing hole size distributions. The different mean values of these distributions do not coincide well with average hole sizes determined by PALS. However, there is a good correlation between distribution parameters and transport coefficients as well as the PALS average hole size for the glassy polymers. The measured cavity sizes better correlate with measured permeabilities than with the mean values of the HSDs. This result follows from neglecting dynamics in the calculation of the hole size distributions. From these results we conclude that the permeation behavior is not determined only by the free volume concentration. The Ps diffusion constants suggest that Ps detects the dynamics of the polymer matrix. The average cavity size from positron annihilation represents a mean value of the hole size distribution.

References and Notes

(1) Nakagawa, T. In *Polymeric Gas Separation Membranes*, 1st ed.; Paul, D. R.; Yampol'skii, Y. P., Eds.; CRC: Boca Raton, FL, 1994; p 399.
(2) Mulder, M. *Basic Principles of Membrane Technology*, Kluwer Academic Publisher: Dordrecht, 1996.
(3) Hofmann, D.; Ulbrich, J.; Fritsch, D.; Paul, D. *Polymer* **1996**, *37*, 4773−4785.
(4) Hofmann, D.; Fritz, L.; Ulbrich, J.; Paul, D. *Polymer* **1997**, *38*, 6145−6156.
(5) Sok, R. M.; Berendsen, H. J. C.; van Gunsteren, W. F. *J. Chem. Phys.* **1992**, *96*, 4699−4704.
(6) Jean, Y. C. *Microchem. J.* **1990**, *42*, 72−102.
(7) Pixton, M. R.; Paul, D. R. In *Polymeric Gas Separation Membranes*, 1st ed.; Paul, D. R.; Yampol'skii, Y. P., Eds.; CRC: Boca Raton, FL, 1994; p 83.
(8) Tanaka, K.; Katsube, M.; Okamoto, K.; Kita, H.; Sueoka, O.; Ito, Y. *Bull. Chem. Soc. Jpn.* **1992**, *65*, 1891−1897.
(9) Kobayashi, Y.; Haraya, K.; Hattori, S. *Polymer* **1994**, *35*, 925−928.
(10) Jean, Y. C.; Yuan, J. P.; Liu, J.; Deng, Q.; Yang, H. *J. Polym. Sci. B: Polym. Phys.* **1995**, *33*, 2365−2371.
(11) Park, J. Y.; Paul, D. R. *J. Membr. Sci.* **1997**, *125*, 23−39.
(12) Trohalaki, S.; DeBolt, L. C.; Mark, J. E.; Frisch, H. L. *Macromolecules* **1990**, *23*, 813−816.
(13) Takeuchi, H.; Roe, R.-J.; Mark, J. E. *J. Chem. Phys.* **1990**, *93*, 9042−9048.
(14) Fritsch, D.; Peinemann, K. V. *J. Membr. Sci.* **1995**, *99*, 29−38.

(15) Fritsch, D.; Avella, N. *Macromol. Chem. Phys.* **1996**, *197*, 701−714.
(16) van Krevelen, D. W. In *Properties of Polymers*, 3rd ed.; van Krevelen, D. W., Ed.; Elsevier: Amsterdam, 1990; p 761.
(17) Bohlen, J.; Wolff, J.; Kirchheim, R. *Mater. Sci. Forum* **1997**, *255*, 393−395.
(18) Dlubek, G.; Stolp, M.; Nagel, C.; Fretwell, H. M.; Alam, M. A.; Radusch, H. J. *J. Phys.: Condens. Matter* **1998**, *10*, 10443−10450.
(19) Kirkegaard, P.; Pedersen, N. J.; Eldrup, M. *Risø-M-2740*, Risø National Laboratory, Denmark, 1989.
(20) Tao, S. J. *J. Chem. Phys.* **1972**, *56*, 5499−5510.
(21) Eldrup, M.; Lightbody, D.; Sherwood, J. N. *Chem. Phys.* **1981**, *63*, 51−58.
(22) Arizzi, S.; Mott, P. H.; Suter, U. W. *J. Polym. Sci. B: Polym. Phys.* **1992**, *30*, 415−426.
(23) Schmidtke, E. Ph.D. Thesis, Christian Albrechts University of Kiel, 2000, in press.
(24) Ferrante, G. *Phys. Rev.* **1968**, *170*, 76−80.
(25) Ciesielski, K.; Dawidowicz, A. L.; Goworek, T.; Jasinska, B.; Wawryszczuk, J. *Chem. Phys. Lett.* **1998**, *289*, 41−45.
(26) Jean, Y. C.; Shi, H. *J. Noncryst. Sol.* **1994**, *172*, 806−814.
(27) Misra, S.; Mattice, W. L. *Macromolecules* **1993**, *26*, 7274−7281.
(28) Greenfield, M. L.; Theodorou, D. N. *Macromolecules* **1993**, *26*, 5461−5472.
(29) Rigby, D.; Roe, R.-J. *Macromolecules* **1990**, *23*, 5312−5319.
(30) Sietsma, J.; Thijsse, B. J. *Phys. Rev. B* **1995**, *52*, 3248−3255.
(31) Hofmann, D.; Fritz, L.; Ulbrich, J.; Paul, D. submitted for publication in *Comput. Theor. Polym. Sci.*
(32) Strobl, G. In *The Physics of Polymers*, 2nd ed.; Strobl, G., Ed.; Springer: Berlin, 1997; p 1.
(33) Mogensen, O. E. In *Springer Series in Chemical Physics*, 1st ed.; Goldanskii, V. I., Schäfer, F. P., Toennies, J. P., Eds.; Springer: Berlin 1995; Vol. 58, p 221.
(34) Nagel, C. Ph.D. Thesis, Christian Albrechts University of Kiel, 1999.
(35) Fritz, L.; Hofmann, D. *Polymer* **1997**, *38*, 1035−1045.
(36) Hirata, K.; Kobayashi, Y.; Ujihira, Y. *J. Chem. Soc., Faraday Trans.* **1996**, *92*, 985−988.
(37) Shantarovich, V. P.; Azamatova, Z. K.; Novikov, Y. A.; Yampolskii, Y. P. *Macromolecules* **1998**, *31*, 3963−3966.

MA990760Y